Stable Middle Miocene seawater isotopes in the eastern North Atlantic Ocean

Katrin Hättig[1], Stefan Schouten[1], Stephen Louwye[2], and Marcel van der Meer[3]

[1]Royal NIOZ
[2]University of Ghent
[3]NIOZ Royal Netherlands Institute for Sea Research

January 24, 2024

Abstract

The Middle Miocene is characterized by a long-term increase in the oxygen isotopes of benthic foraminifera ($\delta^{18}O_{benthic}$). However, it is unclear to what extent this increase reflects changes in seawater isotopes or deep water temperature. We present a high-resolution alkenone hydrogen isotope ($\delta^{2}H_{C37}$) record of the middle Miocene from a core taken at the upper slope edge (about 409 m water depth) of the Porcupine Basin continental margin in the eastern North Atlantic Ocean, Site U1318 of the Integrated Ocean Drilling Program. The $\delta^{2}H_{C37}$ values vary between -174 to -200Importantly, it does not show a long-term increase in surface seawater isotopes ($\delta^{2}H_{SSW}$) during the Middle Miocene Climate Transition. Indeed, when $\delta^{18}O_{benthic}$ is corrected for subsurface temperature, the average bottom seawater oxygen isotopes of 0.9 ±0.2translated into hydrogen isotopes of bottom seawater using the modern open-ocean waterline, it shows an average value of 5.8 +-1.5the $\delta^{2}H_{SSW}$ of 5.2 ±3.1$\delta^{2}H_{C37}$ suggesting relatively small difference between bottom and surface waters. Our results suggest a stable global surface seawater isotope evolution during the Middle Miocene, coupled with a long-term decrease in bottom water temperature.

Hosted file

985128_0_art_file_11792339_s7gs9q.docx available at https://authorea.com/users/717407/articles/702456-stable-middle-miocene-seawater-isotopes-in-the-eastern-north-atlantic-ocean

Hosted file

985128_0_supp_11792340_s7gpx8.docx available at https://authorea.com/users/717407/articles/702456-stable-middle-miocene-seawater-isotopes-in-the-eastern-north-atlantic-ocean

Stable Middle Miocene seawater isotopes in the eastern North Atlantic Ocean

Katrin Hättig[1], Stefan Schouten[1,2], Stephen Louwye[3], Marcel T. J. van der Meer[1]

[1]Department of Marine Microbiology and Biogeochemistry, NIOZ Royal Netherlands Institute for Sea Research, Den Burg, Texel, The Netherlands

[2]Department of Earth Sciences, Utrecht University, Utrecht, The Netherlands

[3]Department of Geology, Ghent University, Ghent, Belgium

Corresponding author: Katrin Hättig (katrin.haettig@nioz.nl)

Key Points:

- No change in stable hydrogen isotopes of surface waters during the Middle Miocene Climate Transition period based on long chain alkenones.
- Bottom seawater isotopes based on corrected oxygen isotopes of benthic foraminifera also show no long-term change during the MMCT.
- Miocene isotope events are reflected by only small $\delta^{18}O$ and $\delta^{2}H$ changes.

Abstract

The Middle Miocene is characterized by a long-term increase in the oxygen isotopes of benthic foraminifera ($\delta^{18}O_{benthic}$). However, it is unclear to what extent this increase reflects changes in seawater isotopes or deep water temperature. We present a high-resolution alkenone hydrogen isotope ($\delta^{2}H_{C37}$) record of the middle Miocene from a core taken at the upper slope edge (about 409 m water depth) of the Porcupine Basin continental margin in the eastern North Atlantic Ocean, Site U1318 of the Integrated Ocean Drilling Program. The $\delta^{2}H_{C37}$ values vary between -174 to -200‰ with an average of -191 ±5‰, similar to modern open-ocean values. Importantly, it does not show a long-term increase in surface seawater isotopes ($\delta^{2}H_{SSW}$) during the Middle Miocene Climate Transition. Indeed, when $\delta^{18}O_{benthic}$ is corrected for subsurface temperature, the average bottom seawater oxygen isotopes of 0.9 ±0.2‰ also show no significant increase. When the latter record is translated into hydrogen isotopes of bottom seawater using the modern open-ocean waterline, it shows an average value of 5.8 ±1.5‰ similar to the $\delta^{2}H_{SSW}$ of 5.2 ±3.1‰ derived from $\delta^{2}H_{C37}$ suggesting relatively small difference between bottom and surface waters. Our results suggest a stable global surface seawater isotope evolution during the Middle Miocene, coupled with a long-term decrease in bottom water temperature.

1 Introduction

The Miocene epoch (23.03-5.33 million years; Cohen et al., 2013) is a globally warm period compared to present day, with CO_2 concentrations varying from pre-industrial to two times higher than at present (Goldner et al., 2014). Most prominent are the Middle Miocene Climate Optimum (MMCO; 16.9-14.7 Ma) and Middle Miocene Climate Transition (MMCT; 14.7–13.8 Ma) where geological, faunal and floral evidence suggest an Antarctic ice sheet retreat and expansion, respectively (e.g., Fielding et al., 2011; Hauptvogel & Passchier, 2012; Levy et al., 2016; Passchier et al., 2011; Pierce et al., 2017; Sangiorgi et al., 2018; Warny et al., 2009). These periods are associated with changes in CO_2 concentrations (Badger et al., 2013; Greenop et al., 2014; Kürschner et al., 2008; Sosdian et al., 2018; Super et al., 2018; Zhang et al., 2013) and characterized by long-term changes in the benthic foraminifera oxygen isotopes ($\delta^{18}O_{benthic}$) (Cramer et al., 2009; Mudelsee et al., 2014; Zachos et al., 2008). Furthermore, the period is also characterized by so-called Miocene oxygen isotope excursions events (Mi-events) (Miller et al., 1991), globally observed short-lived (ca. 100 kyrs) changes in $\delta^{18}O_{benthic}$ (Cramer et al., 2009; Mudelsee et al., 2014), likely representing a decrease in deep-water temperature and/or seawater

isotope changes caused by cryosphere expansion and associated with sea-level variations of tens of meters (John et al., 2011; Levy et al., 2019; Miller et al., 2020; Shevenell et al., 2004, 2008). However, our understanding of ice volume estimates and long-term climate change during this period largely builds on the oxygen isotopes of benthic foraminifera (Miller et al., 2020; Westerhold et al., 2020) a proxy which reflects not only the isotopic composition but also the temperature of seawater (e.g., Savin et al., 1975; Shackleton, 1974). Deep ocean temperature can potentially be constrained by Mg/Ca or carbonate clumped isotopes of foraminiferal shells (Billups & Schrag, 2003; Elderfield et al., 2012; Hou et al., 2023; Lear et al., 2000; Modestou et al., 2020; S. Sosdian & Rosenthal, 2009). Modestou et al. (2020) measured Mg/Ca and Δ_{47} on the same Miocene foraminifera and observed good agreement between the two temperature estimates. Their Δ_{47} temperature change of approximately 2.9 °C recorded over the MMCT suggests a bottom seawater oxygen isotope ($\delta^{18}O_{BSW}$) change of ca. 0.6‰. The Δ_{47} results from Hou et al. (2023) show that Middle Miocene bottom water temperature (BWT) dropped by ca. 5 °C in the Southern Ocean during the MMCT and $\delta^{18}O_{BSW}$ calculations indicate that it was constant over this time, suggesting ice volume was stable. Furthermore, absolute values were close to modern seawater isotopes despite the much warmer global climate. This contrasts earlier estimates of a smaller temperature change during the MMCT and therefore a clear increase in $\delta^{18}O_{SW}$ and ice volume (e.g. Billups & Schrag, 2003; Lear et al., 2000, 2015; Shevenell et al., 2008). Thus, it is not entirely clear how the seawater isotopic compositions evolved over the Middle Miocene due to the different corrections and temperature proxies used to reconstruct bottom water oxygen isotope records from $\delta^{18}O$ benthic foraminiferal records.

Another potential proxy for the isotopic composition of seawater is based on the hydrogen isotopic composition of long chain alkenones ($\delta^{2}H_{C37}$), produced by haptophyte algae. Culture studies show that the hydrogen isotopic fractionation of phototrophic organisms depends on, amongst others, the hydrogen isotopic composition of growth water and salinity (M'boule et al., 2014; Sachs et al., 2016; Schouten et al., 2006; Weiss et al., 2017; Zhang et al., 2009; Zhang & Sachs, 2007). Gould et al. (2019), based on open-ocean suspended particulate organic matter (SPOM), and Mitsunaga et al. (2022), based on core top sediments, show a statistically identical strong relationship between $\delta^{2}H_{C37}$ and the hydrogen isotopic composition of surface water ($\delta^{2}H_{SSW}$). This suggests that in the natural environment, the influence of factors such as temperature, salinity, species composition (e.g., Chivall et al., 2014; M'boule et al., 2014), as

well as light and nutrient availability (Sachs et al., 2017; van der Meer et al., 2015) on stable hydrogen isotope fractionation during biosynthesis might be less important than the hydrogen isotopic composition of seawater. Hättig et al. (2023) used these calibrations to reconstruct δ^2H_{SSW} for the last glacial maximum and found that δ^2H ratios of alkenones are a reproducible paleo-proxy for relative changes in seawater hydrogen isotope composition and fit with other isotope records. Therefore, hydrogen isotopes of alkenones have the potential to produce hydrogen isotope records of surface seawater, independent of temperature.

Here we present a hydrogen isotope record of the $C_{37:2}$ alkenone ($\delta^2H_{C37:2}$) spanning most of the Middle Miocene from 16.60 Ma till 12.75 Ma from a shelf site (Site U1318, ~400 m water depth) in the Porcupine Basin, in the eastern North Atlantic, and compare it to the local benthic foraminiferal $\delta^{18}O$ record previously published by Quaijtaal et al. (2018). The latter record showed the clear impact of the MMCT by a substantial increase in benthic $\delta^{18}O$ of 1‰ in line with the global benthic stack (Westerhold et al., 2020). Furthermore, the Porcupine Basin foraminiferal stable isotope record shows imprints of some Mi-events (Quaijtaal et al., 2018). We reconstructed the oxygen isotopic composition of bottom waters by correcting the $\delta^{18}O_{benthic}$ record for subsurface temperature using TEX_{86} and compared this to the hydrogen isotopic composition of surface seawater reconstructed based on the $\delta^2H_{C37:2}$ record. Our results shed new light on the evolution of seawater isotopes in the eastern North Atlantic during the Middle Miocene.

2 Materials and Methods

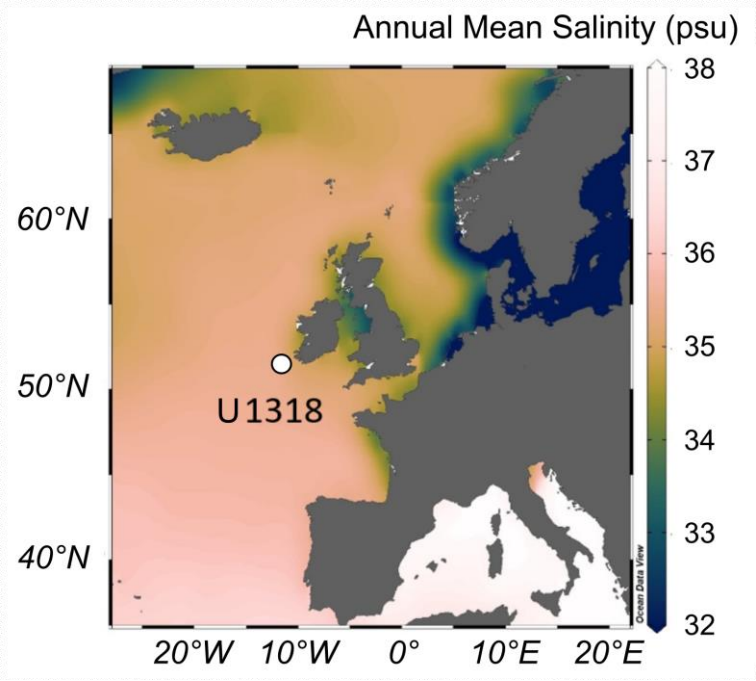

Figure 1. Map of sea surface salinity data from (Zweng et al., 2018) using a scientific colour map from Crameri (2023) showing the sediment core location. U1318 core was drilled in the Porcupine Basin which is at the Northeast Atlantic shelf.

2.1 Geographic Setting

The Integrated Ocean Drilling Program (IODP) drilling site U1318 is located at coordinates 51°26.16'N, 11°33.0'W, with a water depth of 409 meters (Expedition 307 Scientists, 2006). The paleolatitude during the Middle Miocene (~ 15 Ma) was ~47°N (Van Hinsbergen et al., 2015) at a similar water depth as today (Ryan et al., 2009), situated on the upper slope edge of the continental margin within the Porcupine Seabight (Figure 1). The seabight represents a failed rift system that originated during the Middle to Late Jurassic period when the North Atlantic Ocean was being formed. During the Middle Miocene epoch (16-11.7 million years; Cohen et al., 2013), the British Isles were still connected to continental Europe, with no connection to the North Sea (Gibbard & Lewin, 2003). The Porcupine Basin is filled with approximately 12 kilometers of sedimentary deposits ranging from the Late Paleozoic era to the Quaternary period (Ryan et al., 2009). These sediments primarily originate from the Irish and Celtic shelves (Rice et al., 1991). Present-day surface water temperatures (SST) at Site U1318 show a seasonal variation, ranging from ca. 10 °C during winter to around 16 °C during summer (Locarnini et al., 2018). However, at a depth of 409 meters, the water temperature remains constant throughout the

year at approximately 11°C (Locarnini et al., 2018; Sangiorgi et al., 2018). The core location and Porcupine bank is under the influence of the Continental Slope Current (CSC). The CSC transports Eastern North Atlantic Water via the North Atlantic Current (NAC) to the Norwegian Sea (Raddatz et al., 2011). The present-day annual mean salinity of the surface layer (0-50 m) at the core location area is 34.9-35.5 psu (Zweng et al., 2018).

2.2 Age model

To target the Middle Miocene, samples were collected from Site U1318 Hole B (cores 10H-14H and 17X-27X) and Hole C (cores 7H and 8X-10X, Expedition 307 Scientists, 2006) between 92.4 and 247.5 meters composite depth (mcd). The age model for this depth interval is based on integrated bio-, isotope- and magnetostratigraphy, as presented in Quaijtaal et al. (2018). Two hundred forty-five (245) samples were previously analysed for $U_{37}^{K'}$ and TEX_{86} proxies (Sangiorgi et al., 2021) from which 145 samples had sufficient material for stable oxygen and carbon isotopes analysis of the benthic foraminifera *Uvigerina sp.* and *Cibicidoides pachyderma* (Quaijtaal et al., 2018). The Middle Miocene samples consist mainly of greenish-grey clay with total organic carbon content ranging between 0.27–0.70% (Sangiorgi et al., 2021). The samples between 92.4 and 247.5 mcd cover the age interval 12.75–16.60 Ma with an average time resolution of 25 kyrs for stable carbon and oxygen isotope analysis and 17 kyrs for organic geochemistry. To increase the resolution of the organic geochemistry and hydrogen isotope record we extracted 25 additional samples between 98.05 mbsf and 230.42 mbsf following the extraction and fractionation procedures of Sangiorgi et al. (2021). The average time resolution for the extended organic geochemistry record is 14 kyrs and 31 kyrs for the hydrogen isotope record.

2.3 Long-chain alkenones and GDGT analysis

Alkenones and glycerol dialkyl glycerol tetraethers (GDGTs) were extracted and analysed as previously described by Sangiorgi et al.(2021). Furthermore, we re-analysed all GDGT fractions with improved analytical methodology (Hopmans et al., 2016) using an ultra-high performance liquid chromatography/ mass spectrometry (UHPLC/ MS) on an Agilent 1260 Infinity HPLC 230 coupled to Agilent 6130 MSD using two silica BEH HILIC columns (2.1 mm × 150 mm, 1.7 µm 232 thickness) connected in series and maintained at 25 °C. A solvent gradient of hexane/ isopropanol (9:1, v/v) (solvent A) and hexane (solvent B) was used starting with 18% of solvent

A and 82% of solvent B at a constant flow rate of 0.2 ml/ min. The GDGTs were eluted isocratically for 25 min and thereafter solvent A increased in a linear gradient to 30% in 25 min and to 100% of solvent A in the following 30 min. GDGTs were detected in Selective Ion Monitoring (SIM) mode for protonated GDGT molecules $[M+H]^+$. The TEX_{86} index was calculated after Schouten et al. (2007) and the calibration against the average subsurface temperature between 0-200 m (subT) is from Kim et al. (2012) (Equation 1, 2).

$$TEX_{86}^{H} = \log(TEX_{86}) \quad (1)$$

$$subT_{H} = 54.7 * TEX_{86}^{H} + 30.7 \quad (2)$$

The alkenones of the ketone fractions of the 25 additional samples taken in the study were measured using an Agilent 6890N gas chromatograph coupled to a flame ionization detector (GC-FID), equipped with a CP Sil-5 fused silica capillary column (50 m × 0.32 mm, 0.12 µm thickness), to determine the quality of the fraction for further isotope analysis and to calculate the $U_{37}^{K'}$ values (Equation 3) according to (Prahl & Wakeham, 1987). The $U_{37}^{K'}$-based SSTs were calculated with the global core-top calibration of (Müller et al., 1998) (Equation 4).

$$U_{37}^{K'} = \frac{[C_{37:2}]}{[C_{37:2}] + [C_{37:3}]} \quad (3)$$

$$SST = \frac{U_{37}^{K'} - 0.044}{0.033} \quad (4)$$

Hydrogen isotope ratios of alkenones of 124 fractions (99 from the original sample set of Sangiorgi et al, 2021 and 25 additional samples) were measured in duplicate using a gas chromatograph coupled to a Thermo Delta V isotope ratio mass spectrometer via high-temperature conversion reactor (Isolink I) and Conflo IV. The GC was equipped with an RTX–200 60 m column according to Weiss et al. (2019). We report the δ^2H ratio of alkenone $C_{37:2}$ determined by manual peak integration. $C_{37:2}$ appears as the main alkenone peak, while $C_{37:3}$ and C_{38} alkenone peaks are in lower relative abundance and most of the time below minimal intensity for the isotope ratio integration. Daily, before running samples, the H_3^+ factor was measured and the day to day variability was never more than 0.5 ppm/nA, and the performance and stability of the machine was monitored by measuring an n-alkane standard, Mix B (supplied by A. Schimmelmann, Indiana University). Samples were only run when the average difference and standard deviation between online and certified values was less than 5‰. To monitor the system performance squalene and C_{30} n-alkane were co-injected with each sample with measured values

ranging from -161 ±11‰ and -74 ±6‰. The offline predetermined values are -170 ±4‰ for squalene and -79 ±5‰ for C_{30} n-alkane.

2.4 Calculation of seawater isotopes

For the calculation of δ^2H_{SSW} from the hydrogen isotopic composition of $C_{37:2}$ we applied the open–ocean relationship based on surface ocean suspended particulate organic material (SPOM) by Gould et al. (2019):

$$\delta\,^2H_{C37} = 1.48\ (\pm 0.4) \times \delta\,^2H_{SW} - 199\ (\pm 3) \quad <=> \quad \delta\,^2H_{SSW} = \frac{\delta\,^2H_{C37} + 199}{1.48} \tag{5}$$

We reconstructed the oxygen isotopic composition of the bottom seawater ($\delta^{18}O_{BSW}$) from the benthic foraminifera $\delta^{18}O$ data set published in Quaijtaal et al. (2018) which consists of $\delta^{18}O$ values of *Cibicidoides pachyderma* and $\delta^{18}O$ values of *Uvigerina sp* converted to *C. pachyderma*. For the temperature correction we used the updated and extended records of $U_{37}^{K'}$ and TEX^{H}_{86} (Supplement 1). We calculated the $\delta^{18}O_{BSW}$ with the relationship described by Lynch-Stieglitz et al. (1999) as arranged by Cramer et al. (2011) (Equation 6, 7). We report $\delta^{18}O_{BSW}$ values in VSMOW with the accepted conversion value of 0.27‰ (VPDB to VSMOW) (6, 7) (Cramer et al., 2011).

$$t = 16.1 - 4.76 * (\delta^{18}O_{Foram} - (\delta^{18}O_{BSW} - 0.27)) \quad \text{(Cramer et al., 2011)} \tag{6}$$

Rearranged to $\delta^{18}O_{BSW}$:

$$\delta^{18}O_{BSW} = \frac{-16.1 + 4.76 \times \delta^{18}O_{Foram} + t}{4.76} + 0.27 \tag{7}$$

The modern open-ocean relationship between oxygen and hydrogen isotopes is described by Hättig et al. (2023) as the modern open-ocean waterline (MOOWL) and is based on the data sets of Gould et al. (2019); Rohling (2007); Srivastava et al. (2010); Weiss et al. (2019) and the Water isotope Database (2022) managed by Dr. G. Bowen (University of Utah):

$$\delta\,^2H_{sw} = 6.58 \times \delta^{18}O_{sw} - 0.12 \tag{8}$$

3 Results and discussion

3.1 Temperature records

The reanalysis of GDGT fractions of IODP core U1318B using updated methodology (Hopmans et al., 2016) resulted in slightly shifted TEX^{H}_{86} values by on average -0.01 compared to those published by Sangiorgi et al. (2021), with some values changing by up to 0.06 due to the better separation of GDGTs, especially the GDGT-2 peak (Supplement Fig. S1b). In contrast to Sangiorgi et al. (2021), we converted the TEX^{H}_{86} values to subsurface temperature (subT; the average of 0–200 m temperatures as defined by Kim et al. 2012) values as we aim to ultimately use the temperature estimates to correct the $\delta^{18}O_{benthic}$ values (see below). The subT record varies between 13 °C and 21 °C (Fig. 2) and shows the same cooling trends described by Sangiorgi et al. (2021) for the SST inferred from TEX^{H}_{86}. The recalculated BIT index is below 0.3 in all samples, in good agreement with Sangiorgi et al. (2021), suggesting no bias on TEX_{86} values by continental organic matter input (Supplement Fig. S1b). The GDGT-2/ GDGT-3 ratio (Taylor et al., 2013) is relatively constant between 1.7 to 3.2 and implies no remarkable changes in the production depth of GDGTs (Kim et al., 2015; Taylor et al., 2013) as expected in this relatively shallow water location of ca. 409 m depth. The extended $U^{K'}_{37}$-based SST record is on average 4–8 °C higher than the subT estimated from TEX^{H}_{86} with temperatures varying between 25.8–28.9 °C (Fig. 2) and a cooling of ca. 3 °C between 14.6–12.7 Ma. Thus the $U^{K'}_{37}$ reflects a similar temperature trend as TEX^{H}_{86} but with a relatively smaller amplitude, which is surprising as bottom water temperatures typically vary to a smaller degree then surface water temperatures. This difference is likely due to the $U^{K'}_{37}$ reaching its maximum value of 1 (cf Sangiorgi et al., 2021) and thus this proxy is unable to record the substantially warmer SST of >29 °C which may have been present during the first part of the Middle Miocene record.

3.2 Evolution of oxygen isotopes of bottom water

The oxygen isotope ratio of benthic *Cibicidoides pachyderma* as published by Quaijtaal et al. (2018) follows the trend of the global benthic stack (Westerhold et al., 2020, CENOGRID). During the MMCO between 16.6 Ma and 14.59 Ma, the $\delta^{18}O_{benthic}$ signal varies between -0.35‰ and 0.58‰ with an average value of 0.12 ±0.23‰. During the MMCT from 14.59 Ma to 12.75 Ma, values increase as high as 1.43‰. This ca. 1‰ increase is similar to what is observed in the global $\delta^{18}O_{benthic}$ stack record and has until recently been associated with ice volume increase

(Billups & Schrag, 2002; Haq et al., 1987; Rohling et al., 2022). Recent studies, however, suggest a strong bottom water cooling explaining most of the increase in $\delta^{18}O_{benthic}$, and therefore little to no ice volume build up (Hou et al., 2023; Leutert et al., 2021; Meckler et al., 2022; Modestou et al., 2020).

Several Mi-events were tentatively identified based on positive oxygen isotope excursions linked to magnetostratigraphy and palynology changes (Quaijtaal et al., 2014, 2018; Sangiorgi et al., 2021). In particular Mi-events 2, 2a and 3 are likely reflected in the local $\delta^{18}O_{benthic}$ with positive excursions of ca. 0.8‰. The Mi-2a event (ca. 14.8 Ma) is linked to an eustatic sea level fall of ca. 30 m and a cooling of ca. 0.7 ºC in deep waters (John et al., 2011; Miller et al., 2020) and the Mi-3 event (13.8 Ma) is associated with cooling in the deep ocean of 1.2 ºC and ca. 50 m eustatic sea level fall (De Vleeschouwer et al., 2017; Miller et al., 2020) and a pCO_2 decline from ca. 600 ppm to 400-500 ppm (Sosdian & Lear, 2020). The global Mi-4 (Steinthorsdottir et al., 2021) is less pronounced in our local record with a small increase of ca. 0.3‰.

To reconstruct $\delta^{18}O_{BSW}$ from benthic foraminifera we need to reconstruct bottom water temperatures (e.g., Hou et al., 2023; Lear et al., 2015; Modestou et al., 2020). Unfortunately, we were not able to do this using benthic foraminifera. However, the core location is at a rather shallow water depth of ca. 409 m with present day relatively small temperature differences between bottom waters and subsurface (0–200 m) waters of 1–5 °C (Locarnini et al., 2018; Sangiorgi et al., 2021). Therefore, we corrected $\delta^{18}O_{benthic}$ with the subT derived from TEX^{H}_{86}. The obtained $\delta^{18}O_{BSW}$ varies between 0.6 and 1.4‰, a similar range as reconstructed by Hou et al. (2023) for the Middle Miocene at the Southern Hemisphere deep-ocean Site 1168.

Interestingly, our reconstructed bottom water oxygen isotope record shows no decreasing trend between 14.5 Ma and 13.5 Ma and only a minor decrease of ca. 0.2‰ after 13.5 Ma (Figure 2; see Supplement 1 for further discussion). This suggests no major change in seawater isotope compositions after 14.6 Ma at least for this core location in the eastern North Atlantic, in agreement with the suggestion of Sangiorgi et al. (2021) that benthic oxygen isotopes of U1318 are mainly controlled by temperature at this core location.

Regarding the short-term Mi-events, during Mi-2 and Mi-2a the reconstructed $\delta^{18}O_{BSW}$ shows a sharp excursion of 0.3‰ while Mi-3 and Mi-4 show a stepwise increase of 0.2−0.3‰. However, it is difficult to distinguish those events from the large variability in the record which can be up to 0.5‰.

3.3 Evolution of hydrogen isotopes of surface water

The $\delta^2H_{C37:2}$ values of the Middle Miocene sediment record at Site U1318 ranges between -200‰ and -172‰ (Fig. 2c). In contrast to the $\delta^{18}O_{benthic}$ and subT record (Fig. 2d), the $\delta^2H_{C37:2}$ record shows no substantial increase between 14.6 Ma and 12.75 Ma. Between 15.5 Ma and 15.2 Ma $\delta^2H_{C37:2}$ decreases parallel to the $\delta^{18}O_{benthic}$ record from -190‰ to -195‰, followed by a sharp increase to -186‰. But, during the global cooling step and Mi-3 event $\delta^2H_{C37:2}$ increases first continuously from -200‰ at 14.1 Ma to -187‰ at 13.7 Ma, then decreases sharp to -195‰ and continues to vary. Due to the large variability we were not able to rigorously identify the Mi-events in the $\delta^2H_{C37:2}$ record.

The $\delta^2H_{C37:2}$ alkenone record was subsequently converted into a δ^2H_{SSW} record using the calibration of Gould et al. (2019) (Equation 5). This assumes that the alkenones are mainly derived from open–ocean haptophyte species. However, little is known about haptophyte species during the Miocene. The main producer may have been Reticulofenestra (Perch-Nielsen, 1985; Samtleben, 1980), ancestor of the present day open–ocean species Emiliania huxleyi (Gibbs et al., 2013). We observed a typical open-ocean alkenone distribution with a dominant abundance of the $C_{37:2}$ next to C_{38} suggesting that open-ocean haptophytes (Type III; Kleijne, 1993) are the dominant alkenone producers at the time.

Conversion of the $\delta^2H_{C37:2}$ alkenone values resulted in δ^2H_{SSW} values ranging between -1 and +17‰. The average δ^2H_{SSW} for this record is 5.2 ±3.1‰, which is similar to the nearest (ca. 313 km distance from the core site) modern measured δ^2H value of surface seawater, +2.1‰ (Gould, 2019). Similar to the $\delta^2H_{C37:2}$ record there is no decrease in δ^2H_{SSW} after 14.8 Ma, in contrast to the $\delta^{18}O_{benthic}$ and subT records. During the Mi-events, δ^2H_{SSW} seemingly increased by 2−6‰, but these events cannot be clearly distinguished due to the large overall variability, similar to the reconstructed $\delta^{18}O_{BSW}$. Thus, reconstructed δ^2H_{SSW} and $\delta^{18}O_{BSW}$ records both show a lack of any substantial decline in isotopes ratios between 14.6 and 12.75 Ma, although $\delta^{18}O_{BSW}$ does show a small increase after 13.5 Ma. These two independent records thus suggest that this period, the Miocene Climate Transition (MMCT; 14.7–13.8 Ma) was not associated with a substantial change in isotopic composition of seawater in the eastern North Atlantic.

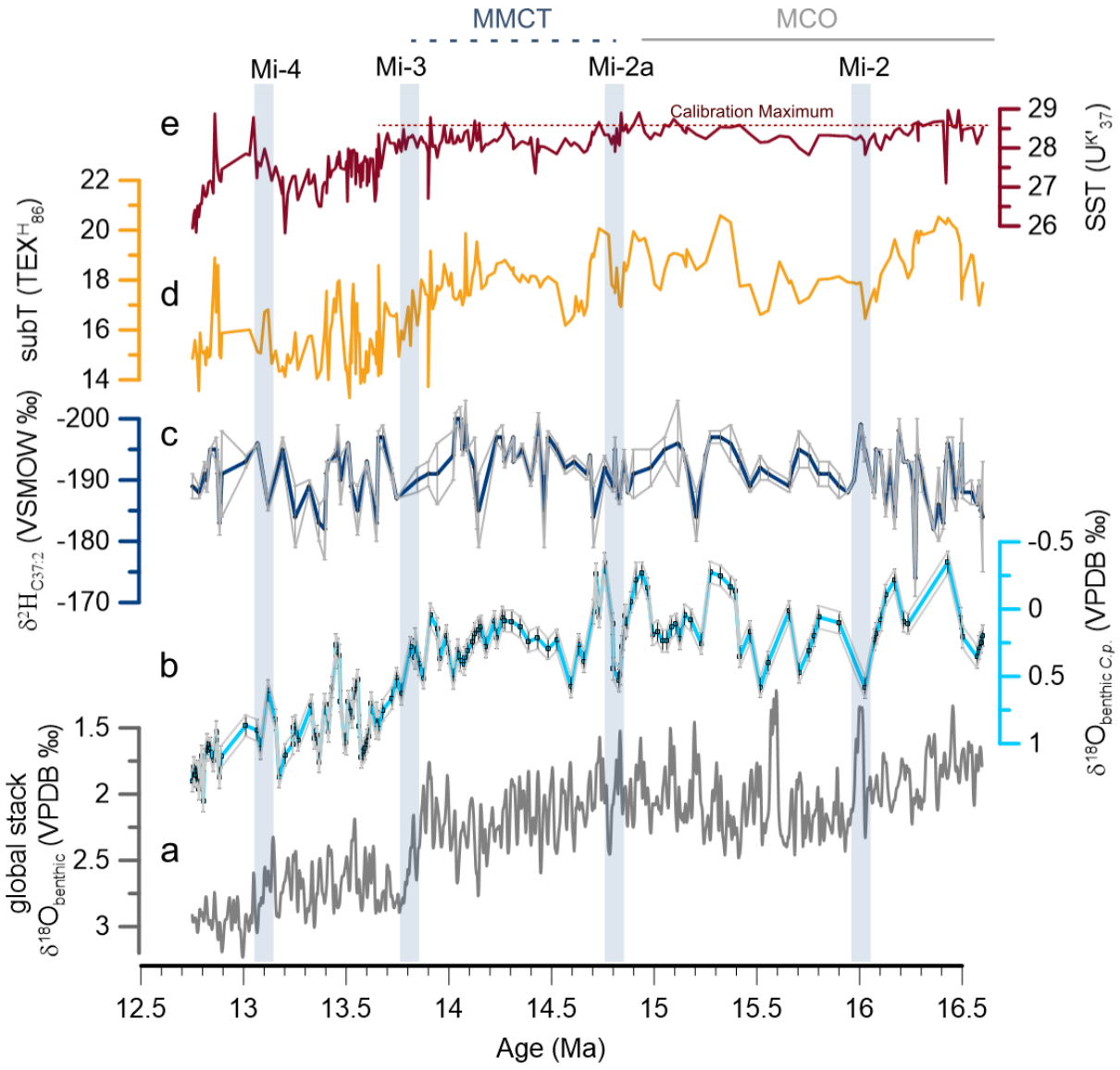

Figure 2. Middle Miocene multiproxy temperature and seawater isotope record, Site U1318. Globally recognized Miocene cooling events (Mi-events; Miller et al., 1991, Steinthorsdottir et al., 2021) are marked with blue bars and were identified by Quaijtaal et al. (2014) based on a sharp increase in $\delta^{18}O_{benthic}$ in combination with palynology and magnetostratigraphy. (a) Global stack $\delta^{18}O$ of benthic foraminifera (CENOGRID, Westerhold et al., 2020); (b) local oxygen isotope data of *Cibicidoides pachyderma* (*C.p.*) (Quaijtaal et al., 2018); (c) δ^2H of long-chain alkenones $C_{37:2}$ (this study); (d) revised subsurface temperature (subT) based on TEX^{H}_{86} index calculated with Kim et al. (2012) (this study); (e) surface temperature (SST) based on $U^{K'}_{37}$ index (Sangiorgi et al., 2021). The age model is presented in Quaijtaal et al., (2018).

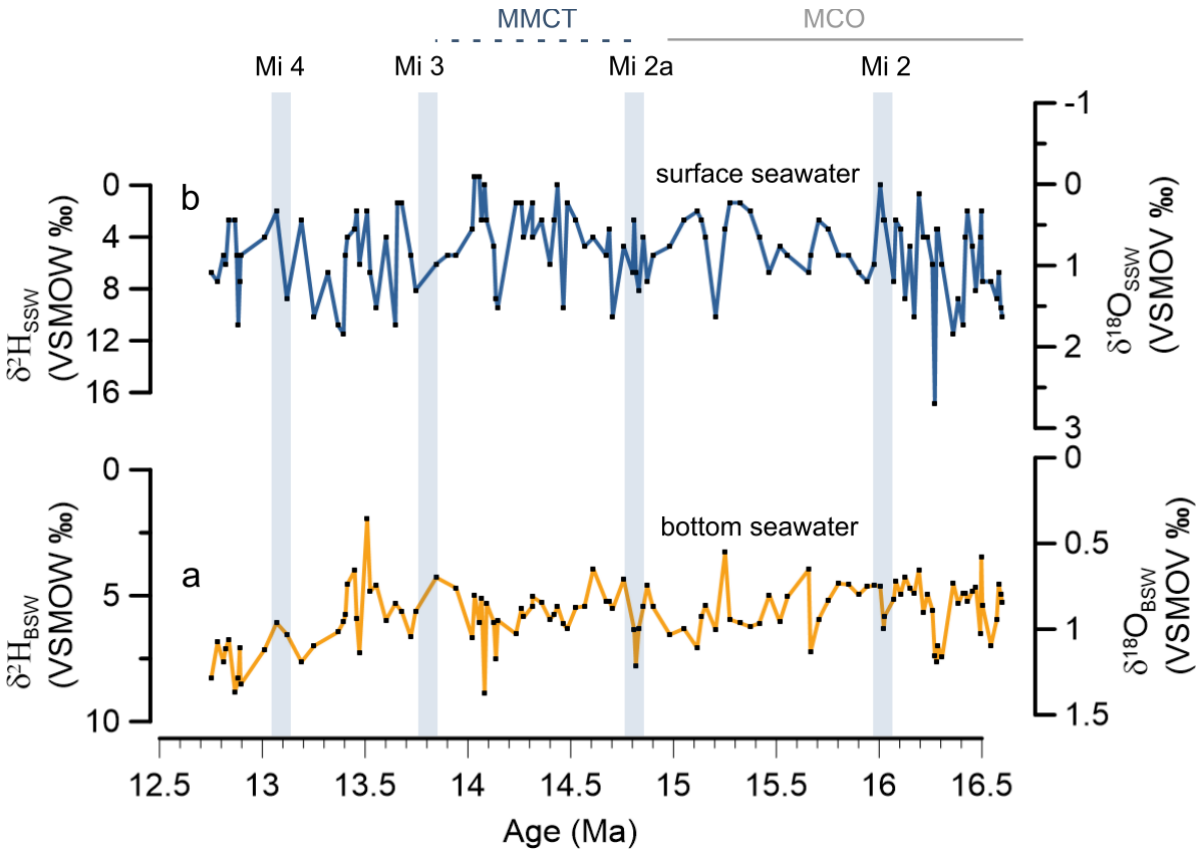

Figure 3. Seawater isotope reconstruction. (a) Bottom seawater isotopes are reconstructed with oxygen isotopes of foraminifera: $\delta^{18}O_{BSW}$ is calculated with Cramer et al., (2011) and subT from the same sediment depth signal. $\delta^{18}O_{BSW}$ was translated with the modern open-ocean waterline (MOOWL) to $\delta^{2}H_{BSW}$. (b) The surface seawater isotope reconstruction is based on hydrogen isotope analysis of C37:2 alkenones, $\delta^{2}H_{SSW}$ is calculated with the SPOM calibration from Gould et al. (2019) and translated to $\delta^{18}O_{SSW}$ with the MOOWL (Equation 8). Global Miocene cooling events (Mi-events; Miller et al., 1991, Steinthorsdottir et al., 2021) are marked with blue bars and are identified by Quaitaal et al. (2014) based on a sharp increase in $\delta^{18}O_{benthic}$ in combination with palynology and magnetostratigraphy.

4 Implications

Our results, based on a novel approach not requiring any temperature correction, clearly show that the MMCT was not associated with a strong change in seawater isotopes, but mainly reflecting a substantial cooling of 4–5 °C in the eastern North Atlantic Ocean. The question arises whether this phenomenon is unique for this location or whether it is a global phenomenon. Interestingly, our results agree with recent studies based on clumped isotope data of benthic foraminifera which suggest higher than previously estimated bottom water temperatures during the MCO and indicate strong bottom water cooling during the MMCT (Hou et al., 2023; Leutert et al., 2021; Meckler et al., 2022; Modestou et al., 2020). Their inferred cooling of ca. 5 °C could

in principle completely explain the global Middle Miocene $\delta^{18}O_{benthic}$ evolution and implies a stable ice volume and thus little to no ice volume buildup (Hou et al., 2023). Our results confirm Middle Miocene stable seawater isotopes suggesting no ice volume buildup. This contrasts geological observations of ice sheet advances during those time periods (e.g., Fielding et al., 2011; Hauptvogel & Passchier, 2012; Levy et al., 2016; Passchier et al., 2011). However, as suggested by Hou et al. (2023) the progressive Neogene Southern Ocean ice volume could be explained by a progressively lowering Antarctic ice sheet height while the ice expands seawards during the Middle Miocene. The total global ice volume might have been stable but the volume to area ratio might have changed (Hou et al., 2023). This million year MMCT cooling caused by the decrease in pCO_2 (Pagani et al., 1999; Super et al., 2018) may thus have led to similar global ice volumes coupled with deep ocean cooling.

Translation of our average reconstructed hydrogen isotopes of surface seawater (δ^2H_{SSW} = 5.2 ±3.1‰) to $\delta^{18}O_{SSW}$ using the MOOWL suggests values of ca. 0.8 ±0.5‰, similar to that in $\delta^{18}O_{BSW}$ = 0.9 ±0.2‰ based on foraminifera. This suggest relatively small differences between bottom and surface seawater isotopes. Furthermore, similar to Hou et al. (2023) the reconstructed surface and bottom seawater isotopes fall in the range of the modern open-ocean seawater isotope composition ($\delta^{18}O$ = -0.5 and 1.5‰, δ^2H = 0-10‰, Le Grande et al., 2006; Rohling et al., 2007; Haettig et al., 2023). This may imply similar ice volumes in the MMCT as those of modern day (Rohling et al., 2022; Hou et al., 2023).

During the Middle Miocene there were several short-lived (ca. 100 kyr) $\delta^{18}O_{benthic}$ increases thought to be associated with bottom water temperature decreases of 0.7–1.2°C and attendant sea-level falls of 20-50 m: Mi-2 (16 Ma), Mi-2a (14.8 Ma), Mi-3 (13.8 Ma), and Mi-4 (13.1 Ma) (Holbourn et al., 2013; Miller et al., 2020). However, both our reconstructed $\delta^{18}O_{BSW}$ and δ^2H_{SSW} values do not consistently show these excursions mainly due to the large overall variability in our records. For our δ^2H_{SSW} record, this variability may be caused by the analytical uncertainty of compound-specific hydrogen isotope analysis, e.g. the analytical reproducibility is ca. 5‰ based on replicate analysis for standards. Furthermore, variable fractionation factors between alkenones and water for different species (e.g., Schouten et al., 2006; M'Boule et al., 2014; van der Meer et al., 2015; Wolhowe et al., 2015) may lead to incorrect estimates of δ^2H_{SSW} while the calibration error between δ^2H_{C37} and δ^2H_{SSW} is also relatively large (root-mean-square error of 5.8‰ for the calibration of Gould et al., 2019), hinting at factors other than δ^2H_{SSW} impacting

δ^2H_{C37} such as light intensity and nutrient availability (e.g., van der Meer et al., 2015; Sachs et al., 2017; Weiss et al., 2017; Wolfshorndl et al., 2019; Wolhowe et al., 2015). Our reconstructed $\delta^{18}O_{BSW}$ may be impacted by incorrect estimations of subsurface water TEX^H_{86} estimates. Furthermore, the $\delta^{18}O_{benthic}$ record may be influenced by diagenetic alteration (e.g., Corfield et al., 1990, Pearson et al., 2001, 2007, Sexton et al., 2006, 2008) and bioturbation (e.g., Hülse et al., 2022). Quaijtaal et al. (2018) did observe minor secondary crystals on the shell walls which might have influenced the isotopic values.

Clearly it would be beneficial to generate hydrogen isotope records from different sites, including equatorial and Southern Ocean sites, to reconstruct the global surface seawater isotope distribution and evolution and potentially disentangle which isotope events (Mi-events) were caused by cooling or a combination of cooling and seawater isotope change. Nevertheless, our results have shown potential for δ^2H_{C37} records in the Cenozoic to provide seawater isotope records which are independent from temperature.

5 Conclusions

We presented a high-resolution Middle Miocene hydrogen isotope record of alkenones from a shelf site (U1318) in the Porcupine basin, in eastern North Atlantic. Our record reflects no long-term changes in surface seawater isotopes during the MMCT. Calculated bottom seawater isotopes based on benthic oxygen isotopes and subsurface TEX^H_{86} temperature correction also indicate no long-term change during this period. This suggests fairly stable seawater isotopes during the MMCT for both bottom and surface waters at this shallow (409 m) site, suggesting no or a very limited ice volume effect on seawater isotopes and indicating that the Miocene Climate Transition was mainly a time of cooling. More independent seawater isotope records of the Atlantic and Pacific Ocean covering the MMCT are needed to confirm if this was a global phenomenon.

Author contribution

All four (co-) authors collectively contributed to the conceptualisation of this study. KH ordered 25 extra samples from IODP, prepared apolar, ketone and polar fractions and analysed alkenones and GDGTs for sea surface temperature. KH analysed the hydrogen isotopic composition of alkenones on the ketone fractions from Sangiorgi et al. (2021) and the extra samples.

Visualisation of research results and original draft preparation was done by KH. SL contributed data. SSc and MTJvdM reviewed and edited the original draft.

Acknowledgments

We thank Dr. Holger Kuhlmann from IODP Bremen Repository for providing samples of U1318. Jort Ossebaar and Ronald van Bommel are thanked for analytical support. We thank Anchelique Mets and Willemijn Quaijtaal for the preparation and storage of apolar, polar and ketone fractions. Devika Varma is thanked for the re-analysis of the polar fractions and integration of GDGT peak areas. This work was carried out under the umbrella of the Netherlands Earth System Science Centre (NESSC). This project has received funding from the European Union's Horizon 2020 research and innovation programme under the Marie Sklodowska-Curie, grant agreement No 847504.

Open Research

All data can be found in the Supplementary Information. Data is also available at PANGAEA repository at xxx. All processed sediment samples are stored at NIOZ, i.e. TLE, apolar, ketone, polar fractions of U1318.

References

Badger, M. P. S., Lear, C. H., Pancost, R. D., Foster, G. L., Bailey, T. R., Leng, M. J., & Abels, H. A. (2013). CO2 drawdown following the middle Miocene expansion of the Antarctic Ice Sheet. Paleoceanography, 28(1), 42–53. https://doi.org/10.1002/palo.20015

Billups, K., & Schrag, D. P. (2002). Paleotemperatures and ice volume of the past 27 Myr revisited with paired Mg/Ca and 18 O/ 16 O measurements on benthic foraminifera . Paleoceanography, 17(1), 3-1-3–11. https://doi.org/10.1029/2000pa000567

Billups, K., & Schrag, D. P. (2003). Application of benthic foraminiferal Mg/Ca ratios to questions of Cenozoic climate change. Earth and Planetary Science Letters, 209(1–2), 181–195. https://doi.org/10.1016/S0012-821X(03)00067-0

Chivall, D., M'Boule, D., Sinke-Schoen, D., Sinninghe Damsté, J. S., Schouten, S., & Van der Meer, M. T. J. (2014). The effects of growth phase and salinity on the hydrogen isotopic composition of alkenones produced by coastal haptophyte algae. Geochimica et Cosmochimica Acta, 140, 381–390. https://doi.org/10.1016/j.gca.2014.05.043

Cramer, B. S., Miller, K. G., Barrett, P. J., & Wright, J. D. (2011). Late Cretaceous-Neogene trends in deep ocean temperature and continental ice volume: Reconciling records of benthic foraminiferal geochemistry (δ18O and Mg/Ca) with sea level history. Journal of Geophysical Research: Oceans, 116(12). https://doi.org/10.1029/2011JC007255

Cramer, B. S., Toggweiler, J. R., Wright, J. D., Katz, M. E., & Miller, K. G. (2009). Ocean overturning since the Late Cretaceous: Inferences from a new benthic foraminiferal isotope compilation. Paleoceanography, 24(4). https://doi.org/10.1029/2008PA001683

Crameri, F.: Scientific colour maps (8.0.0), Zenodo [data set], https://doi.org/10.5281/zenodo.5501399, 2023.

De Vleeschouwer, D., Vahlenkamp, M., Crucifix, M., & Pälike, H. (2017). Alternating Southern and Northern Hemisphere climate response to astronomical forcing during the past 35 m.y. Geology, 45(4), 375–378. https://doi.org/10.1130/G38663.1

Elderfield, H., Ferretti, P., Greaves, M., Crowhurst, S., McCave, I. N., Hodell, D., & Piotrowski, A. M. (2012). Evolution of Ocean Temperature and Ice Volume Through the Mid-Pleistocene Climate Transition. Science, 337(6095), 704–709. https://doi.org/10.1126/science.1221294

Eedition 307 Scientists. (2006). Site U1318. In T. G. Ferdelman, A. Kano, T. Williams, J.-P. Henriet, & The Expedition 307 Scientists (Eds.), Proceedings of the Integrated Ocean Drilling Program (Vol. 307, pp. 1–57). Washington, DC: Integrated Ocean Drilling Program Management International.

Fielding, C. R., Browne, G. H., Field, B., Florindo, F., Harwood, D. M., Krissek, L. A., Levy, R. H., Panter, K. S., Passchier, S., & Pekar, S. F. (2011). Sequence stratigraphy of the ANDRILL AND-2A drillcore, Antarctica: A long-term, ice-proximal record of Early to Mid-Miocene climate, sea-level and glacial dynamism. Palaeogeography, Palaeoclimatology, Palaeoecology, 305(1), 337–351. https://doi.org/https://doi.org/10.1016/j.palaeo.2011.03.026

Gibbard, P. L., & Lewin, J. (2003). The history of the major rivers of southern Britain during the Tertiary. Journal of the Geological Society, 160(6), 829–845. https://doi.org/10.1144/0016-764902-137

Gibbs, S. J., Poulton, A. J., Bown, P. R., Daniels, C. J., Hopkins, J., Young, J. R., Jones, H. L., Thiemann, G. J., O'Dea, S. A., & Newsam, C. (2013). Species-specific growth response of coccolithophores to Palaeocene–Eocene environmental change. Nature Geoscience, 6(3), 218–222. https://doi.org/10.1038/ngeo1719

Gould, J., Kienast, M., Dowd, M., & Schefuß, E. (2019a). An open-ocean assessment of alkenone δD as a paleo-salinity proxy. Geochimica et Cosmochimica Acta, 246, 478–497. https://doi.org/10.1016/j.gca.2018.12.004

Gould, J., Kienast, M., Dowd, M., & Schefuß, E. (2019b). An open-ocean assessment of alkenone δD as a paleo-salinity proxy. Geochimica et Cosmochimica Acta, 246, 478–497. https://doi.org/10.1016/j.gca.2018.12.004

Greenop, R., Foster, G. L., Wilson, P. A., & Lear, C. H. (2014). Middle Miocene climate instability associated with high-amplitude CO2 variability. Paleoceanography, 29(9), 845–853. https://doi.org/10.1002/2014PA002653

Haq, B. U., Hardenbol, J., & Vail, P. R. (1987). Chronology of Fluctuating Sea Levels Since the Triassic. Science, 235(4793), 1156–1167. https://doi.org/10.1126/science.235.4793.1156

Hättig, K., Varma, D., Schouten, S., & Van Der Meer, M. T. J. (2023). Glacial-interglacial sea water isotope change near the Chilean Margin as reflected by δ 2 H of C37 alkenones. 1919–1930. https://doi.org/10.5194/egusphere-2023-1042

Hauptvogel, D. W., & Passchier, S. (2012). Early–Middle Miocene (17–14Ma) Antarctic ice dynamics reconstructed from the heavy mineral provenance in the AND-2A drill core, Ross Sea, Antarctica. Global and Planetary Change, 82–83, 38–50. https://doi.org/https://doi.org/10.1016/j.gloplacha.2011.11.003

Hopmans, E. C., Schouten, S., & Sinninghe Damsté, J. S. (2016). The effect of improved chromatography on GDGT-based palaeoproxies. Organic Geochemistry, 93, 1–6. https://doi.org/10.1016/j.orggeochem.2015.12.006

Hou, S., Stap, L. B., Paul, R., Nelissen, M., Hoem, F. S., Ziegler, M., Sluijs, A., Sangiorgi, F., & Bijl, P. K. (2023). Reconciling Southern Ocean fronts equatorward migration with minor Antarctic ice volume change during Miocene cooling. Nature Communications, 14(1). https://doi.org/10.1038/s41467-023-43106-4

Hülse, D., Vervoort, P., van de Velde, S. J., Kanzaki, Y., Boudreau, B., Arndt, S., Bottjer, D. J., Hoogakker, B., Kuderer, M., Middelburg, J. J., Volkenborn, N., Kirtland Turner, S., Ridgwell, A., (2022). Assessing the impact of bioturbation on sedimentary isotopic records through numerical models, Earth-Science Reviews,234, https://doi.org/10.1016/j.earscirev.2022.104213.

John, C. M., Karner, G. D., Browning, E., Leckie, R. M., Mateo, Z., Carson, B., & Lowery, C. (2011). Timing and magnitude of Miocene eustasy derived from the mixed siliciclastic-carbonate stratigraphic record of the northeastern Australian margin. Earth and Planetary Science Letters, 304(3), 455–467. https://doi.org/https://doi.org/10.1016/j.epsl.2011.02.013

Kim, J.-H., Schouten, S., Rodrigo-Gámiz, M., Rampen, S., Marino, G., Huguet, C., Helmke, P., Buscail, R., Hopmans, E. C., Pross, J., Sangiorgi, F., Middelburg, J. B. M., & Sinninghe Damsté, J. S. (2015). Influence of deep-water derived isoprenoid tetraether lipids on the TEX86H paleothermometer in the Mediterranean Sea. Geochimica et Cosmochimica Acta, 150, 125–141. https://doi.org/https://doi.org/10.1016/j.gca.2014.11.017

Kleijne, A. (1993). Morphology, Taxonomy and Distribution of Extant Coccolithophorids (Calcareous Nannoplankton): Katwijk, The Netherlands (Drukkerij FEBO B.V.).

Kürschner, W. M., Kvaček, Z., & Dilcher, D. L. (2008). The impact of Miocene atmospheric carbon dioxide fluctuations on climate and the evolution of terrestrial ecosystems. www.pnas.org/cgi/content/full/

Lear, C. H., Coxall, H. K., Foster, G. L., Lunt, D. J., Mawbey, E. M., Rosenthal, Y., Sosdian, S. M., Thomas, E., & Wilson, P. A. (2015). Neogene ice volume and ocean temperatures: Insights from infaunal foraminiferal Mg/Ca paleothermometry. Paleoceanography, 2006, 1437–1454. https://doi.org/10.1002/2015PA002833

Lear, C. H., Elderfield, H., & Wilson, P. A. (2000). Cenozoic deep-sea temperatures and global ice volumes from Mg/Ca in benthic foraminiferal calcite. Science, 287(5451), 269–272. https://doi.org/10.1126/science.287.5451.269

Leutert, T. J., Modestou, S., Bernasconi, S. M., & Meckler, A. N. (2021). Southern ocean bottom-water cooling and ice sheet expansion during the middle Miocene climate transition. Climate of the Past, 17(5), 2255–2271. https://doi.org/10.5194/cp-17-2255-2021

Levy, R. H., Meyers, S. R., Naish, T. R., Golledge, N. R., McKay, R. M., Crampton, J. S., DeConto, R. M., De Santis, L., Florindo, F., Gasson, E. G. W., Harwood, D. M., Luyendyk, B. P., Powell, R. D., Clowes, C., & Kulhanek, D. K. (2019). Antarctic ice-sheet sensitivity to obliquity forcing enhanced through ocean connections. Nature Geoscience, 12(2), 132–137. https://doi.org/10.1038/s41561-018-0284-4

Levy, R., Harwood, D., Florindo, F., Sangiorgi, F., Tripati, R., von Eynatten, H., Gasson, E., Kuhn, G., Tripati, A., Deconto, R., Fielding, C., Field, B., Golledge, N., McKay, R., Naish, T., Olney, M., Pollard, D., Schouten, S., Talarico, F., … Zattin, M. (2016). Antarctic ice sheet sensitivity to atmospheric CO2 variations in the early to mid-Miocene. Proceedings of the National Academy of Sciences of the United States of America, 113(13), 3453–3458. https://doi.org/10.1073/pnas.1516030113

Locarnini, M., Mishonov, A., Baranova, O., Boyer, T., Zweng, M., Garcia, H., Reagan, J., Seidov, D., Weathers, K., Paver, C., & Smolyar I. (2018). World Ocean Atlas 2018, Volume 1: Temperature. NOAA Atlas NESDIS 81, 52pp.

Lynch-Stieglitz, J., Curry, W. B., & Slowey, N. (1999). A geostrophic transport estimate for the Florida Current from the oxygen isotope composition of benthic foraminifera. Paleoceanography, 14(3), 360–373. https://doi.org/10.1029/1999PA900001

M'Boule, D., Chivall, D., Sinke-Schoen, D., Sinninghe Damsté, J. S., Schouten, S., & Van der Meer, M. T. J. (2014). Salinity dependent hydrogen isotope fractionation in alkenones produced by coastal and open ocean haptophyte algae. Geochimica et Cosmochimica Acta, 130, 126–135. https://doi.org/10.1016/j.gca.2014.01.029

Meckler, A. N., Sexton, P. F., Piasecki, A. M., Leutert, T. J., Marquardt, J., Ziegler, M., Agterhuis, T., Lourens, L. J., Rae, J. W. B., Barnet, J., Tripati, A., & Bernasconi, S. M. (2022). Cenozoic evolution of deep ocean temperature from clumped isotope thermometry. Science, 377(6601), 86–90. https://doi.org/10.1126/science.abk0604

Miller, K. G., Browning, J. V., John Schmelz, W., Kopp, R. E., Mountain, G. S., & Wright, J. D. (2020). Cenozoic sea-level and cryospheric evolution from deep-sea geochemical and continental margin records. Science Advances, 6(20). https://doi.org/10.1126/sciadv.aaz1346

Miller, K. G., Feigenson, M. D., Wright, J. D., & Clement, B. M. (1991). Miocene isotope reference section, Deep Sea Drilling Project Site 608: An evaluation of isotope and biostratigraphic resolution. Paleoceanography, 6(1), 33–52. https://doi.org/https://doi.org/10.1029/90PA01941

Mitsunaga, B. A., Novak, J., Zhao, X., Dillon, J. A., Huang, Y., & Herbert, T. D. (2022). Alkenone δ2H values – a viable seawater isotope proxy? New core-top δ2HC37:3 and δ2HC37:2 data suggest inter-alkenone and alkenone-water hydrogen isotope fractionation are independent of temperature and salinity. Geochimica et Cosmochimica Acta, 339, 139–156. https://doi.org/10.1016/j.gca.2022.10.024

Modestou, S. E., Leutert, T. J., Fernandez, A., Lear, C. H., & Meckler, A. N. (2020). Warm Middle Miocene Indian Ocean Bottom Water Temperatures: Comparison of Clumped Isotope and Mg/Ca-Based Estimates. Paleoceanography and Paleoclimatology, 35(11). https://doi.org/10.1029/2020PA003927

Mudelsee, M., Bickert, T., Lear, C. H., & Lohmann, G. (2014). Cenozoic climate changes: A review based on time series analysis of marine benthic δ18O records. Reviews of Geophysics, 52(3), 333–374. https://doi.org/10.1002/2013RG000440

Müller, P. J., Kirst, G., Ruhland, G., von Storch, I., & Rosell-Melé, A. (1998). Calibration of the alkenone paleotemperature index U37K′ based on core-tops from the eastern South Atlantic and the global ocean (60°N-60°S). Geochimica et Cosmochimica Acta, 62(10), 1757–1772. https://doi.org/https://doi.org/10.1016/S0016-7037(98)00097-0

Passchier, S., Browne, G., Field, B., Fielding, C. R., Krissek, L. A., Panter, K., & Pekar, S. F. (2011). Early and middle miocene antarctic glacial history from the sedimentary facies distribution in the AND-2A drill hole, Ross sea, Antarctica. Bulletin of the Geological Society of America, 123(11–12), 2352–2365. https://doi.org/10.1130/B30334.1

Perch-Nielsen, K. (1985). Cenozoic Calcareous Nannofossils (H. M. Bolli, J. B. Sanders, & K. Perch-Nielsen, Eds.). Plankton Stratigraphy, Cambridge University Press.

Pierce, E. L., van de Flierdt, T., Williams, T., Hemming, S. R., Cook, C. P., & Passchier, S. (2017). Evidence for a dynamic East Antarctic ice sheet during the mid-Miocene climate

transition. Earth and Planetary Science Letters, 478, 1–13. https://doi.org/https://doi.org/10.1016/j.epsl.2017.08.011

Prahl, F. G., & Wakeham, S. G. (1987). Calibration of unsaturation patterns in long-chain ketone compositions for palaeotemperature assessment. Nature, 330(6146), 367–369. https://doi.org/10.1038/330367a0

Quaijtaal, W., Donders, T. H., Persico, D., & Louwye, S. (2014). Characterising the middle Miocene Mi-events in the Eastern North Atlantic realm: A first high-resolution marine palynological record from the Porcupine Basin. Palaeogeography, Palaeoclimatology, Palaeoecology, 399, 140–159. https://doi.org/10.1016/j.palaeo.2014.02.017

Quaijtaal, W., Tesseur, S., Donders, T. H., Claeys, P., & Louwye, S. (2018). A revised and improved age model for the middle Miocene part of IODP Site U1318 (Porcupine Basin, offshore southwestern Ireland). Geological Magazine, 155(5), 1105–1116. https://doi.org/10.1017/S0016756816001278

Raddatz, J., Rüggeberg, A., Margreth, S., & Dullo, W. C. (2011). Paleoenvironmental reconstruction of Challenger Mound initiation in the Porcupine Seabight, NE Atlantic. Marine Geology, 282(1–2), 79–90. https://doi.org/10.1016/j.margeo.2010.10.019

Rohling, E. J. (2007). Progress in paleosalinity: Overview and presentation of a new approach. Paleoceanography, 22(3), 1–9. https://doi.org/10.1029/2007PA001437

Rohling, E. J., Foster, G. L., Gernon, T. M., Grant, K. M., Heslop, D., Hibbert, F. D., Roberts, A. P., & Yu, J. (2022). Comparison and Synthesis of Sea-Level and Deep-Sea Temperature Variations Over the Past 40 Million Years. Reviews of Geophysics, 60(4). https://doi.org/10.1029/2022RG000775

Ryan, W. B. F., Carbotte, S. M., Coplan, J. O., O'Hara, S., Melkonian, A., Arko, R., Weissel, R. A., Ferrini, V., Goodwillie, A., Nitsche, F., Bonczkowski, J., & Zemsky, R. (2009). Global multi-resolution topography synthesis. Geochemistry, Geophysics, Geosystems, 10(3). https://doi.org/10.1029/2008GC002332

Sachs, J. P., Maloney, A. E., & Gregersen, J. (2017). Effect of light on 2H/1H fractionation in lipids from continuous cultures of the diatom Thalassiosira pseudonana. Geochimica et Cosmochimica Acta, 209, 204–215. https://doi.org/10.1016/j.gca.2017.04.008

Sachs, J. P., Maloney, A. E., Gregersen, J., & Paschall, C. (2016). Effect of salinity on 2H/1H fractionation in lipids from continuous cultures of the coccolithophorid Emiliania huxleyi. Geochimica et Cosmochimica Acta, 189, 96–109. https://doi.org/10.1016/j.gca.2016.05.041

Samtleben, C. (1980). Die Evolution der Coccolithophoriden-GattungGephyrocapsa nach Befunden im Atlantik. Paläontologische Zeitschrift, 54(1), 91–127. https://doi.org/10.1007/BF02985885

Sangiorgi, F., Bijl, P. K., Passchier, S., Salzmann, U., Schouten, S., McKay, R., Cody, R. D., Pross, J., Van De Flierdt, T., Bohaty, S. M., Levy, R., Williams, T., Escutia, C., & Brinkhuis, H. (2018). Southern Ocean warming and Wilkes Land ice sheet retreat during the mid-Miocene. Nature Communications, 9(1). https://doi.org/10.1038/s41467-017-02609-7

Sangiorgi, F., Quaijtaal, W., Donders, T. H., Schouten, S., & Louwye, S. (2021). Middle Miocene Temperature and Productivity Evolution at a Northeast Atlantic Shelf Site (IODP U1318, Porcupine Basin): Global and Regional Changes. C, 36(7). https://doi.org/10.1029/2020PA004059

Savin, S. M., Douglas, R., & Stehli, F. G. (1975). Tertiary marine paleotemperatures. GSA Bulletin, 86(11), 1499–1510. https://doi.org/10.1130/0016-7606(1975)86<1499:TMP>2.0.CO;2

Schouten, S., Ossebaar, J., Schreiber, K., Kienhuis, M. V. M., Langer, G., Benthien, A., & Bijma, J. (2006a). The effect of temperature, salinity and growth rate on the stable hydrogen isotopic composition of long chain alkenones produced by Emiliania huxleyi and Gephyrocapsa oceanica. Biogeosciences, 3(1), 113–119. https://doi.org/10.5194/bg-3-113-2006

Schouten, S., Ossebaar, J., Schreiber, K., Kienhuis, M. V. M., Langer, G., Benthien, A., & Bijma, J. (2006b). The effect of temperature, salinity and growth rate on the stable hydrogen isotopic composition of long chain alkenones produced by Emiliania huxleyi and Gephyrocapsa oceanica. Biogeosciences, 3(1), 113–119. https://doi.org/10.5194/bg-3-113-2006

Sexton, P. F., and P. A. Wilson (2009). Preservation of benthic foraminifera and reliability of deep-sea temperature records: Importance of sedimentation rates, lithology, and the need to examine test wall structure, Paleoceanography, 24, PA2208, doi:10.1029/2008PA001650.

Shackleton, N. J. (1974). Attainment of isotopic equilibrium between ocean water and the benthonic foraminifera geuns Uvigerina: Isotopic changes in the ocean during the last glacial. Colloques Internationaux Du C.N.R.S., 219, 203–210.

Shevenell, A. E., Kennett, J. P., & Lea, D. W. (2004). Middle Miocene Southern Ocean Cooling and Antarctic Cryosphere Expansion. Science, 305(5691), 1766–1770. https://doi.org/10.1126/science.1100061

Shevenell, A. E., Kennett, J. P., & Lea, D. W. (2008). Middle Miocene ice sheet dynamics, deep-sea temperatures, and carbon cycling: A Southern Ocean perspective. Geochemistry, Geophysics, Geosystems, 9(2). https://doi.org/10.1029/2007GC001736

Sosdian, S. M., Greenop, R., Hain, M. P., Foster, G. L., Pearson, P. N., & Lear, C. H. (2018). Constraining the evolution of Neogene ocean carbonate chemistry using the boron isotope pH proxy. Earth and Planetary Science Letters, 498, 362–376. https://doi.org/10.1016/j.epsl.2018.06.017

Sosdian, S. M., & Lear, C. H. (2020). Initiation of the Western Pacific Warm Pool at the Middle Miocene Climate Transition? Paleoceanography and Paleoclimatology, 35(12). https://doi.org/10.1029/2020PA003920

Sosdian, S., & Rosenthal, Y. (2009). Deep-Sea Temperature and Ice Volume Changes Across the Pliocene-Pleistocene Climate Transitions. Science, 325(5938), 306–310. https://doi.org/10.1126/science.1169938

Srivastava, R., Ramesh, R., Jani, R. A., Anilkumar, N., & Sudhakar, M. (2010). Stable oxygen, hydrogen isotope ratios and salinity variations of the surface Southern Indian Ocean waters. Current Science, 99(10), 1395–1399.

Steinthorsdottir, M., Coxall, H. K., de Boer, A. M., Huber, M., Barbolini, N., Bradshaw, C. D., Burls, N. J., Feakins, S. J., Gasson, E., Henderiks, J., Holbourn, A. E., Kiel, S., Kohn, M. J., Knorr, G., Kürschner, W. M., Lear, C. H., Liebrand, D., Lunt, D. J., Mörs, T., … Strömberg, C. A. E. (2021). The Miocene: The Future of the Past. Paleoceanography and Paleoclimatology, 36(4). https://doi.org/10.1029/2020PA004037

Super, J. R., Thomas, E., Pagani, M., Huber, M., O'Brien, C., & Hull, P. M. (2018). North Atlantic temperature and pCO2 coupling in the early-middle Miocene. Geology, 46(6), 519–522. https://doi.org/10.1130/G40228.1

Taylor, K. W. R., Huber, M., Hollis, C. J., Hernandez-Sanchez, M. T., & Pancost, R. D. (2013). Re-evaluating modern and Palaeogene GDGT distributions: Implications for SST

reconstructions. Global and Planetary Change, 108, 158–174. https://doi.org/https://doi.org/10.1016/j.gloplacha.2013.06.011

van der Meer, M. T. J., Benthien, A., French, K. L., Epping, E., Zondervan, I., Reichart, G. J., Bijma, J., Sinninghe Damsté, J. S., & Schouten, S. (2015). Large effect of irradiance on hydrogen isotope fractionation of alkenones in Emiliania huxleyi. Geochimica et Cosmochimica Acta, 160, 16–24. https://doi.org/10.1016/j.gca.2015.03.024

Van Hinsbergen, D. J. J., De Groot, L. V., Van Schaik, S. J., Spakman, W., Bijl, P. K., Sluijs, A., Langereis, C. G., & Brinkhuis, H. (2015). A paleolatitude calculator for paleoclimate studies. PLoS ONE, 10(6). https://doi.org/10.1371/journal.pone.0126946

Warny, S., Askin, R. A., Hannah, M. J., Mohr, B. A. R., Raine, J. I., Harwood, D. M., Florindo, F., & Team, the S. M. S. S. (2009). Palynomorphs from a sediment core reveal a sudden remarkably warm Antarctica during the middle Miocene. Geology, 37(10), 955–958. https://doi.org/10.1130/G30139A.1

Weiss, G. M., Massalska, B., Hennekam, R., Reichart, G. J., Sinninghe Damsté, J. S., Schouten, S., & van der Meer, M. T. J. (2020). Alkenone Distributions and Hydrogen Isotope Ratios Show Changes in Haptophyte Species and Source Water in the Holocene Baltic Sea. Geochemistry, Geophysics, Geosystems, 21(2), 2–16. https://doi.org/10.1029/2019GC008751

Weiss, G. M., Schouten, S., Sinninghe Damsté, J. S., & van der Meer, M. T. J. (2019). Constraining the application of hydrogen isotopic composition of alkenones as a salinity proxy using marine surface sediments. Geochimica et Cosmochimica Acta, 250, 34–48. https://doi.org/10.1016/j.gca.2019.01.038

Weiss, M. G., Pfannerstill, Y. E., Schouten, S., Sinninghe Damsté, S. J., & Van Der Meer, T. J. M. (2017). Effects of alkalinity and salinity at low and high light intensity on hydrogen isotope fractionation of long-chain alkenones produced by Emiliania huxleyi. Biogeosciences, 14(24), 5693–5704. https://doi.org/10.5194/bg-14-5693-2017

Westerhold, T., Marwan, N., Drury, A. J., Liebrand, D., Agnini, C., Anagnostou, E., Barnet, J. S. K., Bohaty, S. M., De Vleeschouwer, D., Florindo, F., Frederichs, T., Hodell, D. A., Holbourn, A. E., Kroon, D., Lauretano, V., Littler, K., Lourens, L. J., Lyle, M., Pälike, H., … Zachos, J. C. (2020). An astronomically dated record of Earth's climate and its predictability over the last 66 million years. Science, 369(6509), 1383–1388. https://doi.org/10.1126/SCIENCE.ABA6853

Wolfshorndl, M., Danford, R., & Sachs, J. P. (2019). 2H/1H fractionation in microalgal lipids from the North Pacific Ocean: Growth rate and irradiance effects. Geochimica et Cosmochimica Acta, 246, 317–338. https://doi.org/10.1016/j.gca.2018.11.027

Wolhowe, M. D., Prahl, F. G., Langer, G., Oviedo, A. M., & Ziveri, P. (2015). Alkenone δD as an ecological indicator: A culture and field study of physiologically-controlled chemical and hydrogen-isotopic variation in C<inf>37</inf> alkenones. Geochimica et Cosmochimica Acta, 162, 166–182. https://doi.org/10.1016/j.gca.2015.04.034

Zachos, J. C., Dickens, G. R., & Zeebe, R. E. (2008). An early Cenozoic perspective on greenhouse warming and carbon-cycle dynamics. Nature, 451(7176), 279–283. https://doi.org/10.1038/nature06588

Zhang, Y. G., Pagani, M., Liu, Z., Bohaty, S. M., & Deconto, R. (2013). A 40-million-year history of atmospheric CO2. Philosophical Transactions of the Royal Society A: Mathematical, Physical and Engineering Sciences, 371(2001). https://doi.org/10.1098/rsta.2013.0096

Zhang, Z., & Sachs, J. P. (2007). Hydrogen isotope fractionation in freshwater algae: I. Variations among lipids and species. Organic Geochemistry, 38(4), 582–608. https://doi.org/https://doi.org/10.1016/j.orggeochem.2006.12.004

Zhang, Z., Sachs, J. P., & Marchetti, A. (2009). Hydrogen isotope fractionation in freshwater and marine algae: II. Temperature and nitrogen limited growth rate effects. Organic Geochemistry, 40(3), 428–439. https://doi.org/10.1016/j.orggeochem.2008.11.002

Zweng, M. M., Reagan, J. R., Seidov, D., Boyer, T. P., Locarnini, R. A., Garcia, H. E., Mishonov, A. V., Baranova, O. K., Weathers, K., Paver, C. R., & I. Smolyar. (2018). World Ocean Atlas 2018, Volume 2: Salinity. A. Mishonov Technical Ed.; NOAA Atlas NESDIS 82, 50pp. In World Ocean Atlas 2018 (Vol. 2:Salinity).

Figure captions

Figure 1. Map of sea surface salinity data from (Zweng et al., 2018) using a scientific colour map from Crameri (2023) showing the sediment core location. U1318 core was drilled in the Porcupine Basin which is at the Northeast Atlantic shelf.

Figure 2. Middle Miocene multiproxy temperature and seawater isotope record, Site U1318. Globally recognized Miocene cooling events (Mi-events; Miller et al., 1991, Steinthorsdottir et al., 2021) are marked with blue bars and were identified by Quaijtaal et al. (2014) based on a sharp increase in $\delta^{18}O_{benthic}$ in combination with palynology and magnetostratigraphy. (a) Global stack $\delta^{18}O$ of benthic foraminifera (CENOGRID, Westerhold et al., 2020); (b) local oxygen isotope data of *Cibicidoides pachyderma* (*C.p.*) (Quaijtaal et al., 2018); (c) $\delta^{2}H$ of long-chain alkenones $C_{37:2}$ (this study); (d) revised subsurface temperature (subT) based on TEX^{H}_{86} index calculated with Kim et al. (2012) (this study); (e) surface temperature (SST) based on $U^{K'}_{37}$ index (Sangiorgi et al., 2021). The age model is presented in Quaijtaal et al., (2018).

Figure 3. Seawater isotope reconstruction. (a) Bottom seawater isotopes are reconstructed with oxygen isotopes of foraminifera: $\delta^{18}O_{BSW}$ is calculated with Cramer et al., (2011) and subT from the same sediment depth signal. $\delta^{18}O_{BSW}$ was translated with the modern open-ocean waterline (MOOWL) to $\delta^{2}H_{BSW}$. (b) The surface seawater isotope reconstruction is based on hydrogen isotope analysis of C37:2 alkenones, $\delta^{2}H_{SSW}$ is calculated with the SPOM calibration from Gould et al. (2019) and translated to $\delta^{18}O_{SSW}$ with the MOOWL (Equation 8). Global Miocene cooling events (Mi-events; Miller et al., 1991, Steinthorsdottir et al., 2021) are marked with blue bars and are identified by Quaitaal et al. (2014) based on a sharp increase in $\delta^{18}O_{benthic}$ in combination with palynology and magnetostratigraphy.